CONTRIBUTIONS OF IMPACT MIXING TO THE SPATIAL DISTRIBUTION OF WATER ICE IN PERMANENTLY SHADED LUNAR SOUTH POLAR CRATERS. P. E. Montalvo[1], M. Hirabayashi[1,2], and D. T. King Jr[1], [1] Department of Geosciences, Auburn University, Auburn AL 36849 USA. [2]Department of Aerospace and Engineering, Auburn University, Auburn AL 36849 USA. **Email:** pem0020@auburn.edu

Introduction: The major regions around the lunar south pole inferred to host water ice are permanently shaded regions [e.g., 1-6]. Most cold traps that currently are interpreted to host water ice are located in latitudes >80˚. A recent study [7] suggests that they may be widely distributed in micro cold traps. On the Moon, water molecules have been transported by multiple processes, such as material mixing [13,14,17] and thermally driven processes [e.g., 8,9], leading to the settlement in regions where the molecules can be thermally stable [e.g., 10-12]. If the surface temperature is below the sublimation temperature of ~110 K in permanently shadowed regions (PSRs), water ice is cold trapped, accumulated, and mixed in the top layer. Among these transport mechanisms, the impact-driven mixing process may have majorly contributed to the re-distribution of water ice [13,14,17]. The magnitude of impact driven mixing has been argued by analyzing the crater population. Given established knowledge about fragment and mixing zones in an emplaced crater, the crater distribution provides a statistical sense of material mixing over the history of a considered area [16,17]. Applying this technique allows for constraining the lateral and vertical distribution of water ice [13-16].

Objectives: The goal of our study is to analyze the spatial distribution of material mixing caused by impact cratering events in localities where surface water ice resides and provide interpretations of the thickness of water ice deposits and their distribution. In this study we focus on three permanently shaded lunar south polar complex craters, Haworth, Shoemaker and Faustini, in order to provide constraints on how water ice material has been processed over time, which is key information for future lunar exploration missions that will intend to sample and use water as a resource.

Methods: Here, we investigate the material mixing depth on permanently shaded floors of the defined three craters by obtaining the crater distributions and by applying a statistical approach [17].

Characterizations of crater distributions: We used ArcGIS CraterTools [18] and data from the Lunar Orbiter Laser Altimeter (LOLA) [19] at pixel resolutions between 5 to 20 m to perform crater counting. The produced crater population is obtained by observing craters that have been emplaced at a given time. The crater distributions on the floors of Haworth, Shoemaker and Faustini are described in Fig. 1A and show a spatial heterogeneity of crater distributions between crater floors, yielding different crater productions.

Statistical characterizations of mixing depths: We analyzed the depth of material mixing using the technique by Hirabayashi et al. [17]. We considered two key mixing factors: (1) material mixing in a breccia lens, and (2) the CSFD in analyzed regions. We only consider the effect of a breccia lens on mixing because in our target regions it is a primary contributor to vertical mixing, in contrast to ejecta blanketing, which influences shallow and lateral mixing [17]. This model characterizes the depth of regolith by introducing an area fraction of the mixed area to the total area, P, at depth, h [17]. P is a function of h and it is given as

$$P = 1 - \exp\{f_{in}(h)\}, \quad (1)$$

where the exponential term of Equation (2) is given as

$$f_{in} = \frac{\xi X \eta \pi}{\eta - 2}\left\{(r_{max}^{in})^{-\eta+2} - \left(\frac{h}{\delta}\right)^{-\eta+2}\right\} - \frac{\xi X \eta \pi}{\eta - 1}\left(\frac{h}{\delta}\right)\left\{(r_{max}^{in})^{-\eta+1} - \left(\frac{h}{\delta}\right)^{-\eta+1}\right\}, \quad (2)$$

where ξ is produced crater CSFD coefficient, X is the non-dimensional produced crater number based on a constant impact flux [e.g., 15,17], η is the production function slope, r_{max}^{in} is the radius of the largest crater whose breccia lens affects the regolith thickness, h is depth in meters, and δ is the depth parameter. Furthermore, our target craters host surface water ice in their crater floors. Because δ depends on the depth to diameter ratio (d/D) [9] and our study focuses on crater diameters ranging ≥400 m to ~ 1 km and ~400 m, we defined δ as 0.21 and 0.17, respectively. We then calculated the material mixing depths at the crater floor scale (Fig. 1B). To determine the lateral distribution of the mixing depth, we also considered smaller gridded areas, 56.25, 25 and 6.25 km^2 (Fig. 2; Fig. 3).

Results: At the crater floor scale, the material mixing depth varies between each target crater (Fig. 1B) and ranges from ~0.8 m to ~3 m at the 99.99% mixing level. Figures 2 and 3, on the other hand, illustrate the upper and lower limits of the mixing depth in the defined gridded areas. The results show vertical and lateral heterogeneity of material mixing ranging from ~7 cm to ~13 m (upper limit) and ~4 cm to ~7 m (lower limit). The highest material mixing depth values are located in areas that mostly contain larger craters compared to smaller ones. In contrast, grids that mostly contain small crater populations show shallower material mixing depths. Our results show that the mixing process strongly depends on the crater

distribution and suggest depths of ~4 cm to ~13 m but deeper mixing with the presence of larger craters.

Assuming that water ice was originally distributed on the top surface [e.g., 1-7], we infer the mixing depth as the water ice distribution and concentration. When multiple large craters are closely placed with each other, the crater production function tends to be higher, which leads to the generation of more craters, and thus water ice material will be distributed at greater depths with lower concentration. The deeper the mixing depth is, the more the water ice materials are distributed.

Discussion: We used crater counting statistics and an analytical model to infer the distribution of water ice laterally and vertically. Our results predicted that the mixing depth and thus the concentration depend on the crater distribution and thus are heterogeneous even on one crater floor. When more craters are placed, the mixing process becomes active, leading to a higher material mixing depth and thus low concentration. Such process mixes water ice throughout the impact bombardment history [20,21].

We finally note that the derived mixing depth in the present model is not consistent with the water ice distribution predicted by remote sensing observations [1-7]. Particularly, while our model predicts a lower water ice density on large craters because of an expected higher mixing depth, remote sensing observations showed the existence of water ice in such areas [6]. We consider this inconsistency to be plausible because surface water ice would likely be transported from other regions and cold trapped after craters are placed. Our model implies that impact-driven mixing lowers the water ice concentration on a surface. Such low-concentration anomalies infer recent water ice transport processes. If this is the case, the time evolution of water ice in these regions would rather be short. This is consistent with discussions that plasma sputtering, and micrometeoroid bombardment would cause short lifetime of water ice on lunar surface [22].

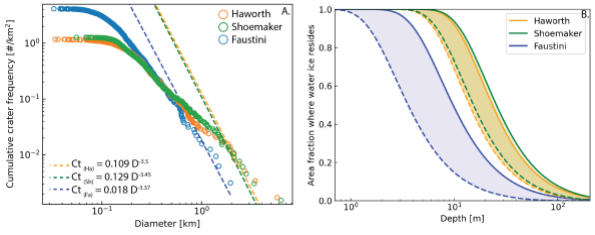

Figure 1. A. Cumulative size frequency distribution (CSFD) plots of target crater floors. Dashed lines are the lunar production and chronology functions [e.g., 23]. B. Profiles showing the material mixing depth. Dashed and solid curves indicate lower and upper limit of material mixing depth, respectively.

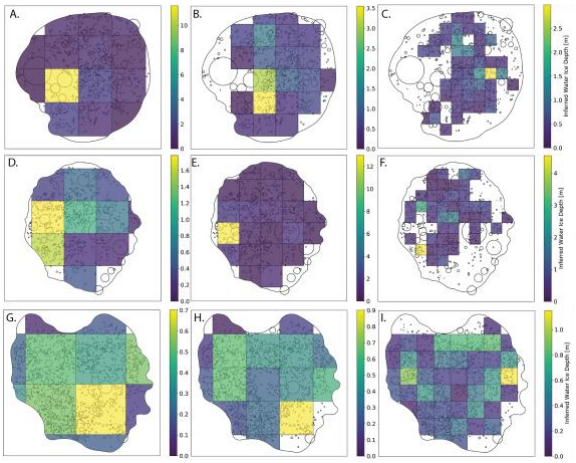

Figure 2. Upper limit of inferred water ice depth distribution. A-C. Haworth. D-F. Shoemaker. G-I. Faustini. Color bars are in meters.

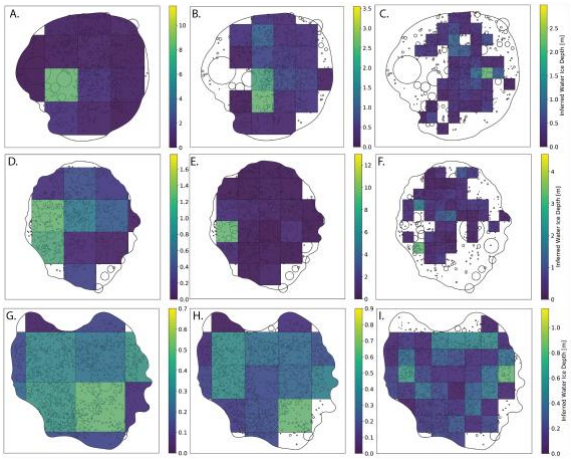

Figure 3. Lower limit of inferred water ice depth distribution.

Acknowledgments: Supported by NASA EPSCoR grant no. 18-EPSCoR R3-0057.

References: [1] Gladstone (2010) *Science*, *330*, 472-476. [2] Hayne et al. (2015) *Icarus*, *255*, 58-69. [3] Mandt et al. (2016) *Icarus*,*273*, 114-120. [4] Fisher et al. (2017) *Icarus*, *292*, 74-85. [5] Patterson et al. (2017) *Icarus*, *283*, 2-9. [6] Li et al. (2018) *PNAS*, *115*, 8907-8912. [7] Hayne et al. (2020) *Nat Astron.* [8] Hayne et al. (2017) *JGRP*, 122, 2371-2400. [9] Stopar et al. (2017) *Icarus*, 298, 34-48. [10] Huang et al. (2017) *JGRP*, 122, 1158-1180. [11] Moores (2016) *JGRP*,121,46-60. [12] Prem (2015) *Icarus*, 255, 148-158. [13] Prem et al. (2018) *Icarus*, 299, 31-45. [14] Xiao and Werner (2015) *JGRP*,120, 2277-2292. [15] Hirabayashi et al. (2017) *Icarus*, 289, 134-143. [16] Costello et al. (2020) *JGRP*, 125, e2019JE006172. [17] Hirabayashi et al. (2018) *JGRP*, 123, 527-543. [18] Kneissl et al. (2011) *PSS*, 59, 1249-1254. [19] Smith et al. (2010) *SSR*, 150, 209-241. [20] Cannon and Britt (2020) *Icarus*, 347, 113778. [21] Cannon et al. (2020) *GRL* 46, e2020GL088920. [22] Farrell et al. (2019) *GRL 46*, 8680-8688.[23] Neukum et al. (2001) *SSR*, 96, 55-86.